Monatshefte für Chemie 133, 859–872 (2002)

Monatshefte für Chemie
Chemical Monthly

Influence of Nanoporosity and Roughness on the Thickness-Dependent Coercivity of Iron Nanonetworks

Syed A. M. Tofail[1], **Zakia I. Rahman**[1,*], **Abdur M. Rahman**[2], and **Razeeb K. U. Mahmood**[1]

[1] Department of Physics and Materials and Surface Science Institute, University of Limerick, Limerick, Ireland
[2] Department of Electronic and Computer Engineering and Materials and Surface Science Institute, University of Limerick, Limerick, Ireland

Summary. We have studied the coercivity of magnetic nanonetworks as a function of thickness, nominal pore diameter, and surface/interface roughness in the thickness range of approximately 2 to 45 nm where a *Néel*-type domain wall has been theoretically predicted. Such magnetic nanonetworks have been prepared by sputtering iron on the walls of commercially available porous nanochannel alumina (NCA) membranes. The thickness dependence of coercivity has also been studied on films deposited on surface-oxidized Si and glass subtrates. These substrates are essentially non-porous and much smoother than NCAs. Our investigation shows that the coercivity of films deposited on Si and glass depends on the spatial fluctuation of thickness which arises from the roughness of the apparently smooth substrates. On the other hand, NCAs are found to be inherently quite rough, and films on NCAs show a complex thickness dependence which arises from the interplay between surface/interface roughness, domain pinning due to porosity, surface anisotropy, surface torques, and oxidation of the iron films. It was found that the growing films on NCA substrates led to partial filling up of the pore entrance, thereby reducing its effective diameter. The film growth also affects the roughness of the film, which in turn affects its coercivity. We propose a model for the thickness dependence of coercivity based on the pore fill-up geometry considering the effective pore diameter and the critical thickness at which the pore will be completely filled up. Experimental results on coercivity with thickness variation of iron network deposited on NCA generally agree with the suggested model.

Keywords. Nanostructures; Magnetic properties; Iron film; Porosity; Surface roughness.

Introduction

Fabrication of patterned structures on the nanometer scale in two or three dimensions require a suitable pattering technique such as optical or electron beam lithography, or alternatively the use of nanotemplates. Depending on the method of

* Corresponding author. E-mail: zakia.rahman@ul.ie

patterned matrix formation, either a positive or a negative nanostructured network can be obtained [1]. Many earlier works on patterned magnetic nanostructures have been focused on magnetic information storage to achieve higher recording density beyond 100 Gbits/in^2. Studying patterned media is also relevant to the understanding of fundamental magnetic phenomena. For example, *Cowburn et al.* [2] have found that investigations of the nucleation of magnetic domains and homogeneity in conventional magnetic thin films are greatly facilitated by an anti-dot array. Anisotropy barriers and the effect of domain wall pinning on hysteresis behaviour are two other examples of what can be studied from patterned nanostructures [3].

It has been reported that templated nanostructured networks of iron have shown a coercivity increase of two orders of magnitude at around 10–20 nm film thickness as compared to similar films on continuous substrates [4]. These nanonetworks were grown on the top of the walls of porous anodized alumina (commonly known as nano-channel alumina, NCA) to form a contiguous nanonetwork. The width of the pore wall varied between 15–75 nm, depending on the pore size of the alumina template. The coercivity increase is attributed to the tendency of the magnetization of the deposit near the pores to align perpendicular to the film plane, thus acting as a energy barrier for domain wall movement [5]. The whole range of the thickness dependence of the coercivity of the templated iron film is, however, far from being well understood. In order to understand the effect of porous or rough substrates it is important to gather knowledge on the film morphology originating from fabrication history and its impact on the coercivity behaviour. In this article we have attempted to study this problem from the existing theory of the thickness dependence of the coercivity of ferromagnetic materials deposited on non-porous substrates by incorporating porosity in the substrate and surface roughness in the growing film on the top of this substrate. The coercivity (H_c) of sputter-deposited ferromagnetic films is greatly influenced by sputtering conditions and magnetic layer thickness. H_c is defined as the reverse field necessary to bring residual magnetization back to zero. This is critical in determining the amount of information that can be recorded in a given area as well as the stability of these data bits with respect to long-term storage [1]; higher coercivity is desirable for such applications.

The coercivity of the ferromagnetic films depends on thickness and porosity [6], level of oxidation [7], and substrate roughness [8]. Sputtering conditions can control some of these factors. The film thickness is of primary influence on the coercivity as this factor determines both domain wall energy and domain wall type. A domain wall separates two oppositely magnetized domains and consists of a transition layer of characteristic width and energy associated with its formation and existence. In the case of an ideally smooth magnetic film it can be assumed that the magnetization of such a film should be reversed by the parallel displacement of an 180° domain wall which is parallel to the easy magnetization axis of the film so that the energy of the domain wall is a function of displacement. In Fig. 1 such a case of domain wall displacement is shown. In this case, the magnetization direction in region 1 is in the direction of applied magnetic field, and the domain wall in this region grows at the expense of the domain in region 2. For a sufficiently thick films ($D \ll t$; D: domain wall width, t: film thickness), a *Bloch*-type domain wall

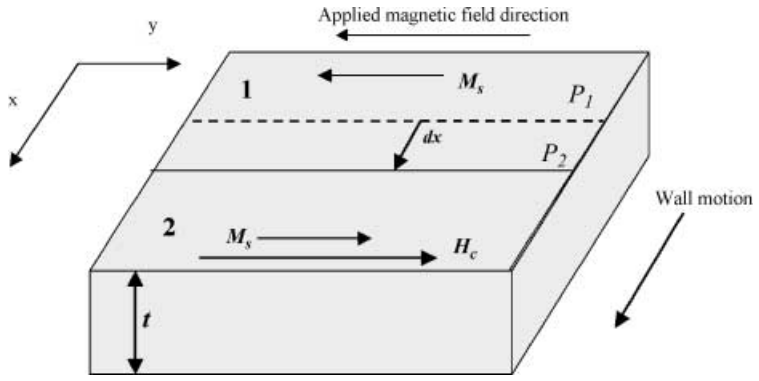

Fig. 1. Parallel displacement of a 180° domain wall from position P_1 to position P_2 in a ferromagnetic film due to an applied magnetic field [9]

can exists [9] in which the magnetization component is perpendicular to the domain wall. In this case, H_c shows the well-known $t^{-4/3}$ dependence as calculated by *Néel* [10]:

$$H_c \propto t^{-4/3} \tag{1}$$

Néel, however, has also pointed out that below a certain critical film thickness the *Bloch* wall will become energetically unfavourable, and the magnetization component will be directed parallel to the domain wall. In this situation, a *Néel*-type domain wall will from ($t \ll D$). *Sohoo* [9] has found that coercivity is independent of thickness and varies according to Eq. (2) where dt/dx is the spatial fluctuation of film thickness.

$$H_c \propto \frac{dt}{dx} \tag{2}$$

For an ideally smooth film on an ideally smooth substrate, dt/dx can be considered to be independent of the film thickness, and hence Eq. (2) should be valid for the thickness range where *Néel*-type domain walls are energetically favourable. If porosity is introduced in this hypothetical substrate, it will render the overlying film to be porous along with the fact that the pore dimensions (diameter and pore wall width) will be a function of the film thickness. This is important in determining the final coercivity of the deposit, as porosity can act as pinning sites for the domain wall, thereby restricting its motion and increasing the coercivity. Recent advances in lithography technique have allowed cutting regular holes into the ferromagnetic films and to investigate the influence of such holes on the magnetic properties of the film. As mentioned before, NCA membranes are also used, as they provide a ready-to-use template to introduce such porosity in the ferromagnetic film [4, 11]. The pores in such templates, as has been discussed elsewhere [11], are often random in geometry (size and distribution) and lack long-range order. In addition, NCA templates exhibit quite high surface roughness. Since all these parameters can influence coercivity, any study on the coercivity behaviour of ferromagnetic films grown on such templates should carefully consider the surface characteristics of the template.

Results and Discussions

Thickness dependent coercivity of films on continuous substrates

Figure 2 shows the thickness dependence of the coercivity of iron films deposited on nonporous substrates, *e.g.* glass and Si; the coercivity values of these two systems showed little difference. Experimental coercivity data followed the relation $H_c = H_0 t^{-0.75}$, where $H_0 = 2\alpha K_1/M_s$ is the anisotropy field, K_1 is the anisotropy constant, M_s is the saturation magnetisation, $\alpha = 0.48$ for random orientation of crystallites in three-dimensions [14], and t is the film thickness. A similar inverse power law dependence of the coercivity on the film thickness with an exponent value of $n = 0.4 \pm 0.1$ was found for Co films deposited on Cu buffered (111) Si by *Min et al.* [8]. The coercivity relationship along with a coercivity lower than the anisotropy field (564 Oe for iron) of the continuous films indicates that the reversal process is governed predominantly by domain wall motion rather than coherent rotation [3]. The inverse power law dependence has been explained by *Min et al.* in terms of the roughness of the ferromagnetic film [8]. For the thickness range studied, the walls were expected to be of *Néel*-type, which means that coercivity should be a function of dt/dx. The observed non-zero exponent n was believed to be due to the variation of film thickness dt/dx as a function of t. If the substrate roughness is small compared to the film thickness, then the root mean square thickness fluctuation should approximately be the sum of the interface widths of the bare substrate and the film-substrate system. Assuming a decrease in film roughness with increasing in film thickness, they suggested that the proposed decrease in the local roughness with deposition of Co could cause the coercivity to decrease by changing the magnetostatic and anisotropy energies [8].

In Fig. 3, the thickness dependence of the roughness as measured from AFM topographies and normalized to their correlation length is shown. The data were fitted using the empirical relation $\sigma/\xi = at^b$, where σ is the roughness and ξ the correlation length measured from AFM. Below 7.5 nm film thickness, the constant a changes its value from 2 to 0.009 for Si and from 3.5 to .009 for glass. The

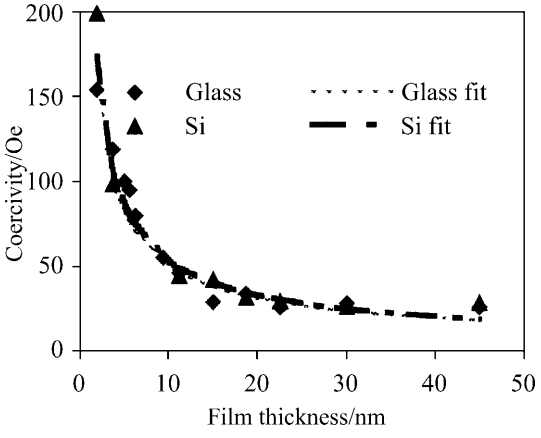

Fig. 2. Thickness dependent coercivity variation of polycrystalline iron films deposited on nonporous substrates, *e.g.* glass and Si

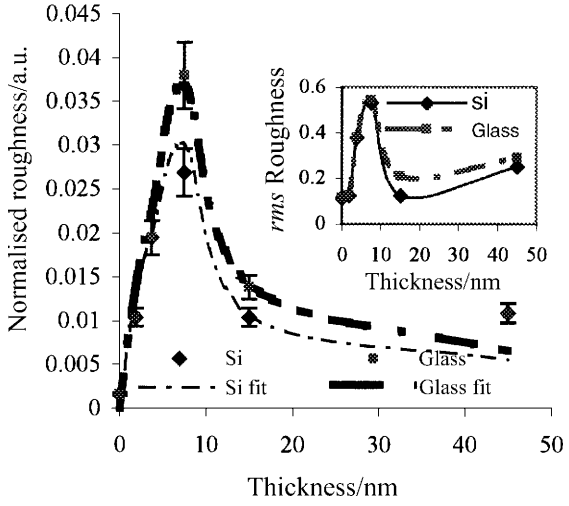

Fig. 3. Thickness variation of the normalized roughness of iron films deposited on non-porous substrates (Si and glass); inset: thickness variation of root mean square roughness of the same set of samples

exponent b changes its sign at this film thickness and assumes a value 0.6 for Si and 0.7 for glass. If we consider the film roughness variation as the spatial fluctuation of film thickness, *i.e.* $\mathrm{d}t/\mathrm{d}x = \sigma/\xi$, then Eq. (2) qualitatively describes the thickness dependence of coercivity in terms of the film roughness.

Thickness dependent coercivity of films on NCA templates

NCA templates are inherently quite rough; this roughness, in turn, has been found to be a function of the pore dimension of the templates [15]. The determination of the spatial fluctuation of film thickness $\mathrm{d}t/\mathrm{d}x$ will therefore be complicated by the presence of porosity and, it should depend on the variation of film thickness, too. This problem can be approached in a much more convenient way if we consider the pore fill-up geometry as shown in Fig. 4. In an earlier report, we have shown the cross-sectional TEM view of a similar deposit on a porous template [11] and found that such a deposition is always associated with a certain degree of pore filling as well as pore capping. The extent to which this will happen depends on the pore diameter, the geometry of the pore opening and, most importantly, on the thickness of the overlying deposit [13]. It should be mentioned that the templates employed for this work are mainly intended for use as filtration membranes to retain oversized particles or organisms. This particular application of the templates has dictated the structure of the membranes, and the pores are tapered along the cross-section. The pore size specified by the manufacturer is only available at the filtration side of the membranes and, as evident from the cross-sectional views so far described, these pores are conical rather than cylindrical (Fig. 4). Closer observation reveals a typical trickling of the iron oxide deposit down the sidewalls of these conical pore openings. The overflow deposit down the sidewalls ends up at a finite distance below the pore entrance.

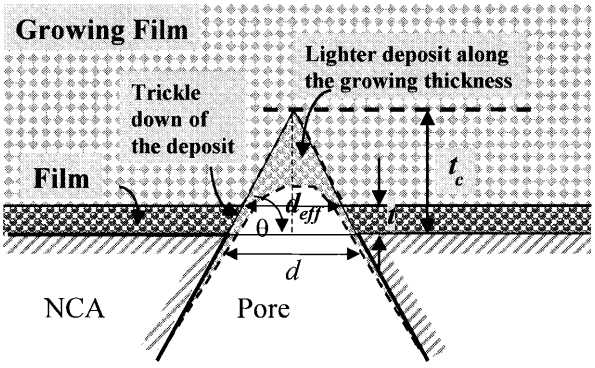

Fig. 4. Schematic diagram of filling of a typical tapered pore with nominal entrance diameter d as a result of deposition of film of thickness t; the critical thickness at which the overlying film will completely cover up the pore is denoted by t_c, whereas d_{eff} is the effective pore diameter at a given thickness and θ the angle the lateral growth of the film subtends to the pore entrance

The growth of the sputter deposited layer over the top of the magnetic layer is also important as it indicates the critical thickness where the pore will be completely filled up by the overlying deposit. A linear overgrowth of the film from the point of inflexion of the conical pores can be noticed which continues up to a certain critical thickness t_c beyond which there is no discontinuity in the overgrown layer. Figure 5 is just a redraw of Fig. 4 ignoring the trickle effect of the deposit; spatial discontinuity in the deposit due to the porous template can be noticed from this diagram. The spatial variation of thickness as well as the spatial variation of

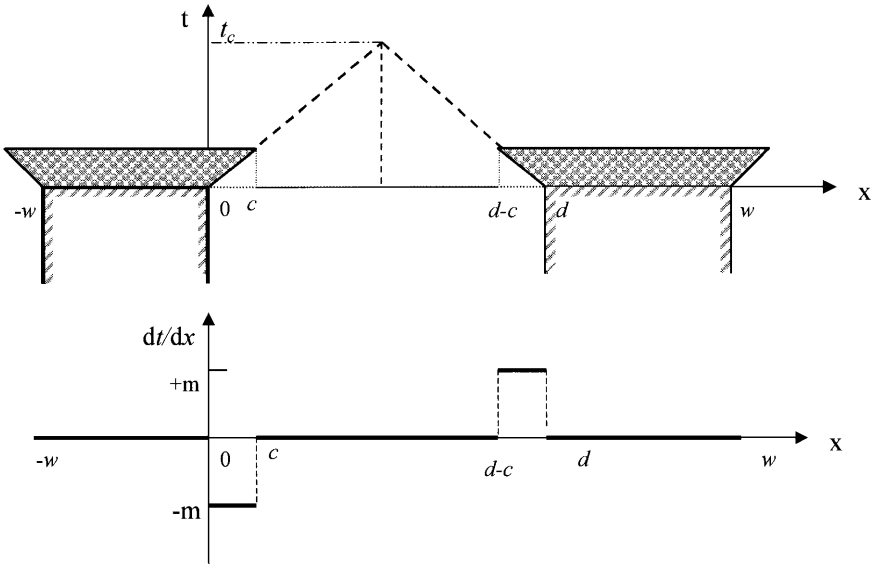

Fig. 5. Spatial variation of thickness and slope of the thickness profile (dt/dx) of an ideal smooth film on a porous substrate; the lateral extent of pore fill-up of the film is denoted by c; w: pore wall width, m: slope of the thickness profile

the slope due to thickness variation of an ideal flat film is also shown in Fig. 5. Assuming that the pores with nominal diameter d are partially filled up by an overlying film of thickness t, the pore diameter at the top of the deposit is given by Eq. (3) where c is the lateral extent of pore fill-up as described in Fig. 5.

$$d_{\text{eff}} = d - 2c \tag{3}$$

On the other hand, the critical thickness t_c for complete filling of the pores will depend on the angle θ that the deposit subtends with the nominal pore diameter. Clearly, c achieves its maximum when $\theta = 0$ and its minimum when $\theta = \pi/2$; a small change $\Delta\theta$ will change c by Δc, and t_c will be reduced by an amount of Δt_c. Then, from geometric relationships and after suitable manipulation, we get $\Delta t_c/t_c = \tan\Delta\theta/\tan\theta$. As $\Delta t_c \to t_c$ when $\Delta\theta \to 0$, $t_c = d\Delta\theta/2$. Also, $\Delta\theta$ corresponds to an equivalent change in the film thickness Δt, resulting in $\Delta\theta = \tan\theta = \Delta t/\Delta c$ and, finally, in Eq. (4).

$$t_c = \frac{d\Delta t}{2\Delta c} \tag{4}$$

This means that the critical thickness at which a conical pore in a template will be completely filled up by the overlying deposit is directly proportional to the pore diameter and the deposited layer thickness and inversely proportional to the lateral extent of pore fill-up by the deposit. For example, a film with $t = 12$ nm and $c = 8$ nm will completely cover a cylindrical pore with 200 nm nominal diameter at $t_c = 150$ nm. This can be verified from Ref. [11], where the conical pores are almost filled up by the amorphous deposit at ~150–175 nm. For a similar type of deposition, t_c can be calculated for 20 and 100 nm nominal pore diameter to be 15 and 75 nm, respectively. This means that continuous film-type behaviour should start from 150, 75, and 15 nm with nominal pore diameters of 200, 100, and 20 nm, respectively.

It can also be shown that $\Delta c \to d/2$ as $\Delta t \to t_c$, so that $c = dt/2t_c$, which means that for a given pore diameter the lateral extent of pore fill-up is a linear function of thickness. Substituting the value of c in Eq. (3) and rearranging affords Eq. (5) which gives the thickness dependence of the pore diameter of a film grown on a porous substrate.

$$d_{\text{eff}} = d\left(1 - \frac{t}{t_c}\right) \tag{5}$$

Mathematically, the thickness profile along the x-axis as can be expressed as

$$\begin{aligned} f(x) = t &= m(c - x) && \text{for} \quad 0 < x < c \\ &= 0 && \text{for} \quad c \le x < d - c \\ &= m(x - (d - c)) && \text{for} \quad d - c \le x < d \\ &= -m(d - c) && \text{for} \quad d \le x < d + w \end{aligned} \tag{6}$$

In Eq. (6), $m = 2t_c/d$ is the slope of the thickness profile along the x-axis. Similarly, the slope of the film thickness profile variation can be expressed as follows:

$$\begin{aligned} f'(x) = \mathrm{d}t/\mathrm{d}x &= -m \quad \text{for} \quad 0 \le x < c \\ &= 0 \quad \text{for} \quad c \le x < d - c \\ &= m \quad \text{for} \quad d - c \le x < d \\ &= 0 \quad \text{for} \quad d \le x < d + w \end{aligned} \tag{7}$$

If we consider that $w = d/2$, we can expand Eq. (7) into a *Fourier* series:

$$\frac{\mathrm{d}t}{\mathrm{d}x} = \sum_{n=1}^{\infty} \left(1 - (-1)^n \cos\frac{d}{2}\left(1 - \frac{t}{t_c}\right)n\pi\right) \frac{8t_c}{3n\pi d} \sin n\pi x \tag{8}$$

Taking the root mean square value over the span between $x = 0$ and $x = 3$, we obtain

$$\frac{\mathrm{d}t}{\mathrm{d}x} = 0.707 \sum_{n=1}^{\infty} \left(1 - (-1)^n \cos\frac{d}{2}\left(1 - \frac{t}{t_c}\right)n\pi\right) \frac{4t_c}{3n\pi d} \tag{9}$$

Equation (9) describes the thickness dependence of the spatial variation of film thickness for ferromagnetic films on a template with 200 nm pores. This simplified relationship becomes much more complicated with the introduction of a rough film on a porous substrate with considerable roughness. We then have to modify Eqs. (7) and (8) by considering the root mean square roughness, σ, of the film as follows:

$$\begin{aligned} f(x) &= m(c - x) + \sigma \quad \text{for} \quad 0 \le x < c \\ &= 0 \quad \text{for} \quad c \le x < d - c \\ &= m(x - (d - c)) + \sigma \quad \text{for} \quad d - c \le x < d \\ &= -m(d - c) + \sigma \quad \text{for} \quad d \le x < d + w \end{aligned} \tag{10}$$

and

$$\begin{aligned} f'(x) = \mathrm{d}t/\mathrm{d}x &= -m + \sigma' \quad \text{for} \quad 0 \le x < c \\ &= 0 \quad \text{for} \quad c \le x < d - c \\ &= m + \sigma' \quad \text{for} \quad d - c \le x < d \\ &= \sigma' \quad \text{for} \quad d \le x < d + w \end{aligned} \tag{11}$$

where $\sigma' = \mathrm{d}\sigma/\mathrm{d}x$ is the spatial fluctuation of film roughness.

We can expand Eq. (11) into a *Fourier* series as:

$$\begin{aligned} \frac{\mathrm{d}t}{\mathrm{d}x} = {} & \sigma'\left(\frac{2c}{3} - 1\right) + \sum_{1}^{\infty} \frac{2c\sigma'}{3n\pi} \sin n\pi c \cos n\pi x \\ & - \sum_{1}^{\infty} \frac{2c\sigma'}{3n\pi} \left(2m\left(1 - (-1)^n \cos n\pi \frac{d_{\mathrm{eff}}}{2}\right) - \sigma'(1 - (-1)^n)\right) \sin n\pi x \end{aligned}$$

Since c is very small, the middle term may be ignored; averaging between $x=0$ and $x=3$ then affords

$$\frac{\mathrm{d}t}{\mathrm{d}x} = \sigma'\left(\frac{2c}{3}-1\right) - 0.707\sum_{1}^{\infty}\frac{2c\sigma'}{3n\pi}\left(\frac{2t_\mathrm{c}}{d}\left(1-(-1)^n\cos n\pi\frac{d}{2}\left(1-\frac{t}{t_\mathrm{c}}\right)\right)\right.$$
$$\left. - \sigma'(1-(-1)^n)\right) \tag{12}$$

We can then modify Eq. (2) for the *Néel* wall zone as

$$H_\mathrm{c} \propto \sigma'\left(\frac{2c}{3}-1\right) - 0.707\sum_{1}^{\infty}\frac{2}{3n\pi}\left(\frac{2t_\mathrm{c}}{d}\left(1-(-1)^n\cos n\pi\frac{d}{2}\left(1-\frac{t}{t_\mathrm{c}}\right)\right)\right.$$
$$\left. - \sigma'(1-(-1)^n)\right)$$

or

$$(H_\mathrm{c})_\mathrm{roughness} \propto \sigma'\left(\frac{2t}{3t_\mathrm{c}}(d-1)\right) - 0.707$$
$$\sum_{1}^{\infty}\frac{2}{3n\pi}\left(\frac{2t_\mathrm{c}}{d}\left(1-(-1)^n\cos n\pi\frac{d}{2}\left(1-\frac{t}{t_\mathrm{c}}\right)\right) - \sigma'(1-(-1)^n)\right) \tag{13}$$

For 20 nm pores, $d \approx w$ rather than $2w$ [4]; Eq. (12) can therefore be modified according to Eq. (14)

$$\frac{\mathrm{d}t}{\mathrm{d}x} = \sigma'\left(\frac{t}{2t_\mathrm{c}}(d-1)\right) - 0.707\sum_{1}^{\infty}\frac{4t_\mathrm{c}}{n\pi d}\cos\frac{\mathrm{d}}{2}\left(1-\frac{t}{t_\mathrm{c}}\right)n\pi \tag{14}$$

which finally affords

$$(H_\mathrm{c})_\mathrm{roughness} \propto \sigma'\left(\frac{t}{2t_\mathrm{c}}(d-1)\right) - 0.707\sum_{1}^{\infty}\frac{4t_\mathrm{c}}{n\pi d}\cos\frac{d}{2}\left(1-\frac{t}{t_\mathrm{c}}\right)n\pi \tag{15}$$

In addition to roughness there will be two other opposing factors working on the magnetization reversal in such systems: domain wall pinning and domain wall nucleation. Whereas porosity in the pinning model hinders domain wall motion and thus increases coercivity, it can also act as a nucleation centre for the nucleation of a domain wall and thereby decrease coercivity.

Hilzinger and *Kronmüller* [16] have considered the pinning of the curved domain walls by randomly distributed defects, and the coercivity was found to depend on $\rho^{1/2}$ for weak pinning and on $\rho^{2/3}$ for strong pinning (ρ: density of inclusions/voids/pores). More recent theories suggest the following conditions for domain wall pinning: $3f/2\pi\gamma\delta < 1$ for weak pinning and $3f/2\pi\gamma\delta > 1$ for strong pinning (f: maximum restoring force a pinning centre can exert on a domain wall, γ: domain energy per unit area, δ: domain wall thickness) [17, 18].

The restoring force can be calculated by using the *Néel* model for unpaired spins at the surface of a nonmagnetic precipitate [19]. If we assume cylindrical pores, the restoring force then can be calculated as $f = 0.5(M_\mathrm{s}^2 N_\mathrm{d})(V_\mathrm{p}/r)$ where V_p

is the volume of the pore, N_d is the demagnetizing field associated with a cylindrical pore ($\approx 1/3$), and r is the radius of the pore. From the volume of the frustum in Fig. 4 it can be concluded that the pore volume at a given thickness t of the film is

$$V_p = \frac{\pi}{12} d^2 \left(1 - \left(1 - \frac{t}{t_c}\right)^3\right) t_c \tag{16}$$

Hence,

$$f = \frac{\pi}{36} M_s^2 \left(1 - \left(1 - \frac{t}{t_c}\right)^3\right) dt_c \tag{17}$$

Taking $\gamma \approx 2\,\mathrm{erg/cm^2}$ and $\delta \approx 6\times10^{-5}\,\mathrm{cm}$ for bulk iron, we can rewrite the condition for strong or weak pinning as $2\times10^9(1-(1-t/t_c)^3)dt_c > 1$ for strong pinning and $2\times10^9(1-(1-t/t_c)^3)dt_c < 1$ for weak pinning. Figure 6 shows the variation of pinning strength with thickness for films deposited on templates with three different nominal pore diameters. Clearly these pore diameters fall within the range where only weak pinning on the domain wall movement is to be expected.

For the coercivity field in the case of weak domain pinning, *Gaunt* [17] suggested

$$H_c = \frac{0.258 f^2 \rho}{M_s \gamma} \tag{18}$$

The number of voids which are intersected by a single domain wall is roughly estimated to be $N^{2/3}$ [20], so that there are $\rho = N^{2/3}/D'$ voids in a unit volume which leads to a decrease in the magnetostatic energy (D': equilibrium separation of domain walls). If a domain wall bisects a pore of diameter d, the free pole areas are divided into regions of opposite polarity [20], thus reducing the magnetostatic

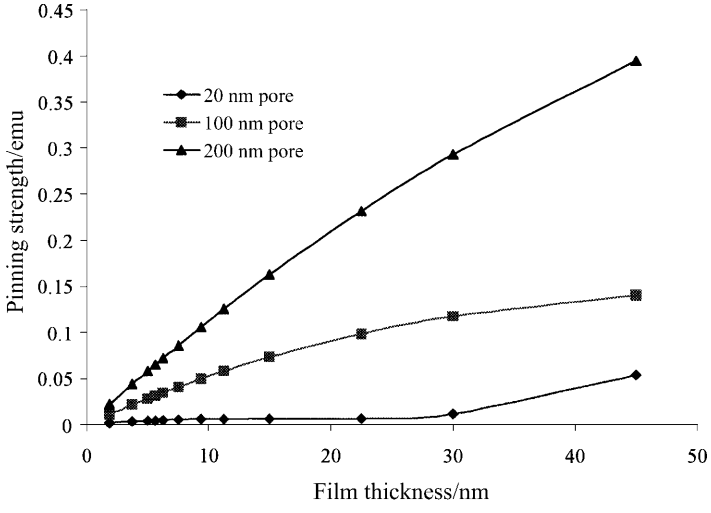

Fig. 6. Variation of domain wall pinning strength due to porosity as a function of thickness

energy to about half the value of that associated with the void. The decrease in total magnetostatic energy can then be found from the condition $N^{2/3} \cdot \Delta E_{ms} \geq \gamma$, where ΔE_{ms} is the decrease in magnetostatic energy due to the presence of one pore ($\Delta E_{ms} = 1/4 M_s^2 N_d V_p$). The equilibrium spacing of the domain wall is given as $D' = (\gamma t / C M_s^2)^{1/2}$ where t is the film thickness and C is a numerical constant that depends on the type of domain. Hence, we can calculate the number of the voids/pores/inclusions per unit volume as

$$\rho = \frac{144 C^{1/2} \gamma^{1/2}}{\pi M_s} \cdot \frac{t^{-1/2}}{d^2 \left(1 - \left(1 - \frac{t}{t_c}\right)^3\right) t_c} \tag{19}$$

Combining Eqs. (17), (18), and (19) we obtain

$$H_c = \frac{0.258 C^{1/2} M_s^2}{9 \gamma^{1/2}} \left(1 - \left(1 - \frac{t}{t_c}\right)^3\right) t_c t^{-1/2}$$

or

$$(H_c)_{pinning} \propto \left(1 - \left(1 - \frac{t}{t_c}\right)^3\right) t_c t^{-1/2} \tag{20}$$

This is shown in Fig. 7 where the normalized coercivity (H_c) is plotted as a function of film thickness for three different pore sizes.

When considering the coercivity of the iron film, we have to take into account all factors at the same time. Combining contributions of film roughness and domain wall pinning due to porosity on the top of a nonporous substrate, we obtain the qualitative relationship

$$H_c \propto (H_c)_{nonporous} (H_c)_{roughness} (H_c)_{pinning} \tag{21}$$

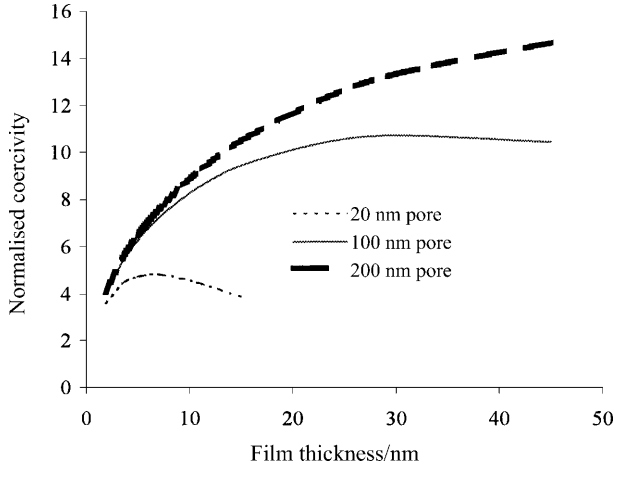

Fig. 7. Normalized coercivity as a function of thickness for templates with three different pore sizes according to the domain wall pinning model

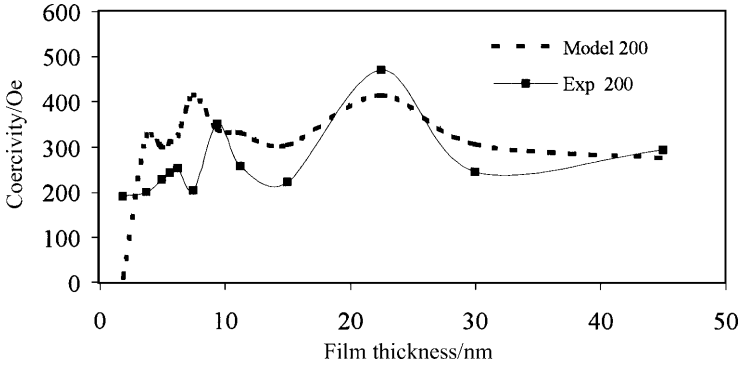

Fig. 8. Thickness dependent coercivity of iron films on NCA templates with 200 nm nominal pore diameters; broken lines: pore fill-up model, dotted lines: experimental values

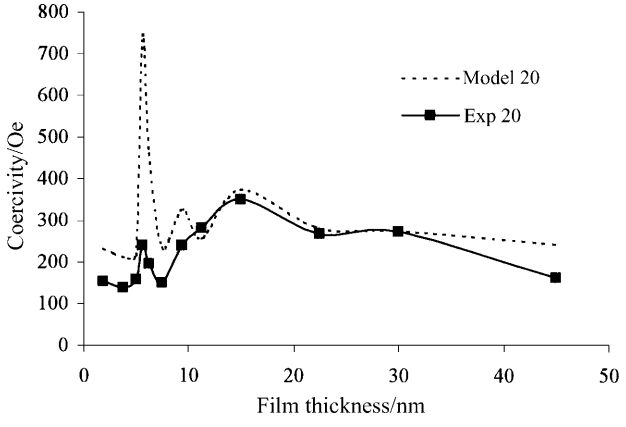

Fig. 9. Thickness dependent coercivity of iron films on NCA templates with 20 nm nominal pore diameters; broken lines: pore fill-up model, dotted lines: experimental values

where $(H_c)_{nonporous}$ is the coercivity of similar films deposited on a nonporous substrate. Figure 2 shows that $(H_c)_{nonporous}$ varies with $t^{-0.701}$. Taking this into account and using coercivity relations from Eqs. (13) and (20) for 200 nm templates and Eqs. (15) and (20) for 20 nm templates, the thickness dependence of coercivity of films deposited on such templates is as presented in Figs. 8 and 9, respectively. The theoretical values generally agree with the experimental values (solid curves).

An exact quantitative relationship is, however, difficult to establish due to the statistical nature of template pore size, pore wall width distribution, and the surface roughness of the film. In the low thickness region, films exhibited lower coercivity than predicted due to the increasing influence of superparamagnetic particles. Throughout the discussion we have ignored the contributions of surface torque and anisotropy energy as well as that of oxidation. These can influence the coercivity, especially in the low thickness region.

Conclusions

We have studied the effect of porosity and roughness on the thickness dependence of the coercivity of thin iron films in the thickness range where *Néel*-type domain wall can exist. Porous alumina templates were used to introduce porosity in the overlying film. We have developed a model on the basis of the obstruction to the domain wall motion due to the presence of pores and surface roughness in the iron film and compared this with both theoretical and experimental observations for iron films deposited on ideal pore-free smooth substrates. The model generally explains the experimental observations on the thickness-dependent coercivity of iron films deposited on nanochannel alumina substrates.

Experimental

Nanonetworks of polycrystalline iron were prepared by RF-diode sputtering of a 6″ iron target (99.95% purity) at 4 mtorr Ar pressure and 400 W sputtering power on commercially available NCA membranes [12] as substrates. The target-to-substrate distance for sputtering was kept constant at 15 cm and the base pressure below 2×10^{-7} mbar. NCA membrane templates are available with three nominal pore diameter sizes (20, 100, and 200 nm); these templates were used for deposition of iron films. Figure 10 shows a typical atomic force microscope (AFM) topography of such a template with 20 nm nominal pore diameter. The pores were found to exhibit a *Gaussian* distribution [13]. When any film is deposited on the pore walls of such templates, it produces a contiguous nanonetwork which can be considered as a negative or anti-dot nanostructured matrix. The presence of an underlying porous template introduces porosity in the overlying network of deposited films. Using similar deposition parameters, iron films were deposited on substrates that do not have any porosity such as surface oxidized (100) Si and glass substrates.

The thickness of the films was measured from cross-sectional TEM on continuous films on Si; surface roughness was determined using a Topometrix™ atomic force microscope (AFM) with an Explorer™ head in the non-contact mode. Hysteresis loops of the samples were determined using a vibrating sample magnetometer (VSM) with a maximum applied field of 3 kOe. The magnetic field was applied along the macroscopic film plane. Coercivity was measured as a function of layer thickness (2–45 nm) from the respective hysteresis loops.

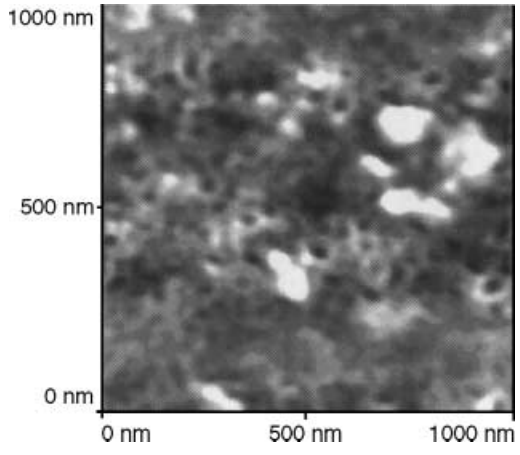

Fig. 10. Typical AFM topography of an NCA membrane with 20 nm nominal pore diameter

Acknowledgements

This project is funded by the Higher Education Authority (HEA), Ireland.

References

[1] Tofail SAM, Rahman IZ, Rahman MA (2001) Appl Organomet Chemistry **15**: 373
[2] Cowburn RP, Adeyeye AO, Bland JAC (1997) Appl Phys Letter **70**: 2309
[3] Tofail SAM, Rahman IZ, Rahman MA (2001) Thickness and Pore Size Dependence of Coercivity for Nanonetwork of Iron Produced by Template Synthesis. Presented at the MMM 2001, Seattle, Washington, Nov 12–16, 2001, to be published in J Appl Phys 2002
[4] Barnard JA, Fujiwara N, Inturi VR, Jarratt JD, Scharf TW, Weston JL (1996) Appl Phys Lett **69**: 2758
[5] Butera A, Weston JL, Barnard JA (1997) J Appl Phys **81**: 7432
[6] Hong M, Gyorgi EM, van Dover RB, Nakahara S, Bacon DD, Gallagher PK (1986) J Appl Phys **59**: 551
[7] Kim YK, Oliviera M (1993) J Appl Phys **74**: 1233
[8] Min H-G, Kim S-H, Li M, Wedding JB, Wang G-C (1998) Surface Science **400**: 19
[9] Sohoo RF (1965) Magnetic Thin Films. Harper & Row, New York, p 142
[10] Néel L (1956) J Phys Rad **17**: 250
[11] Tofail SAM, Rahman IZ, Rahman MA, Newcomb S, Sutton D (2002) J Magn Magn Mat (in press)
[12] Anopore^{TM} Whatman Inc.
[13] Tofail SAM (2002) Patterned Magnetic Nanonetworks on Nanochannel Alumina Templates. PhD Thesis, University of Limerick
[14] Sellmyer DJ, Shan ZS (1997) Magnetic Hysteresis in Novel Nanostructured Films. In: Hadjipanayis GC (ed) Magnetic Hysteresis in Novel Magnetic Materials. Kluwer, Netherlands, pp 419–451
[15] Tofail SAM, Rahman IZ, Rahman MA (2001) Templating for the Fabrication of Nanostructured Network of Iron, Proc 1st IEEE Conference on Nanotechnology (IEEE-NANO 2001), Hawaii, USA, Oct 28–31, 2001, pp 223–228
[16] Hilzinger HR, Kronmüller H (1977) Physica **86-8B**: 1365
[17] Gaunt P (1983) Philos Mag B **48**: 261
[18] Gaunt P (1986) J Appl Phys **59**: 4129
[19] Néel L (1944) Cahiers de Physique **4**: 21
[20] Chikazumi S (1997) Physics of Ferromagnetism. Oxford, p 463

Received October 16, 2001. Accepted (revised) January 11, 2002